Supporting Information for

Development of Actin Dimerization Inducers Inspired by Actin-depolymerizing Macrolides

Moeka Itakura,[1] Didik Huswo Utomo,[1,2] and Masaki Kita [1,*]

[1] *Graduate School of Bioagricultural Sciences, Nagoya University, Furo-cho, Chikusa, Nagoya 464-8601, Japan*

[2] *Bioinformatics Research Center, Indonesian Institute of Bioinformatics, Malang, Jawa Timur 65162, Indonesia*

Correspondence and requests for materials should be addressed to M. K.
(email: mkita@agr.nagoya-u.ac.jp)

(18 pages)

Contents

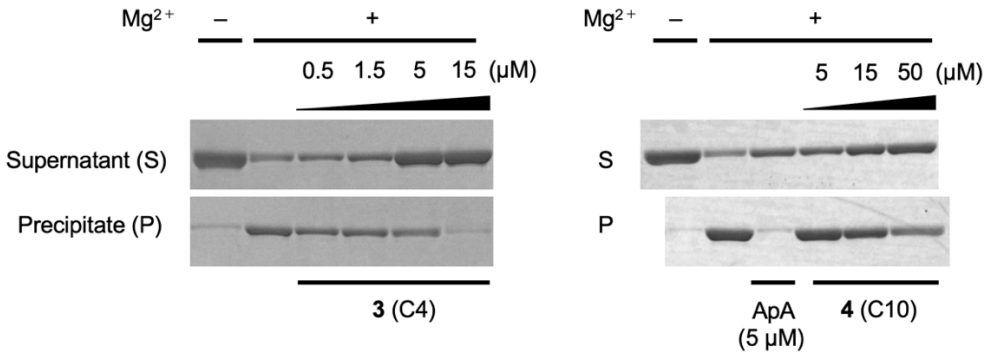

Figure S1. *In vitro* F-actin sedimentation assay. Filamentous (F-) actin (3 μM as a monomer) was precipitated by ultracentifugation after treatment with ApA and its side-chain dimer analogs **3** and **4**. Proteins in the supernatant (S) and precipitate (P) were analyzed by SDS-PAGE and detected with CBB stain.

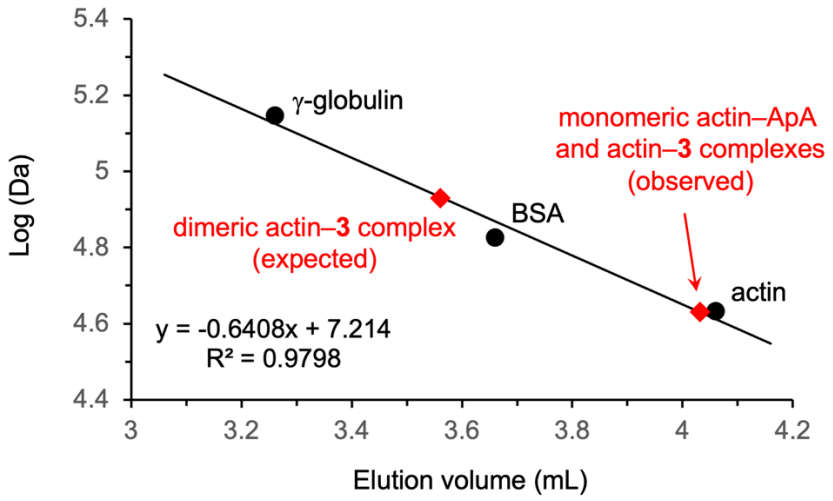

Figure S2. Estimation of the molecular weight of the actin–**3** complex based on gel permeation HPLC analysis. Column, TSKgel SuperSW3000 (ϕ 4.6 × 300 mm). Buffer, 50 mM PIPES·K (pH 6.8), 100 mM KCl, 10 mM $MgCl_2$. Temp., 12 °C. The column was calibrated using protein standards, and a standard curve is shown in the graph. The calculated molecular weight of the monomeric actin–ApA and actin–**3** complexes eluted as a single peak was 44~45 kDa (see Fig. 2a), which are consistent with their actual molecular weights.

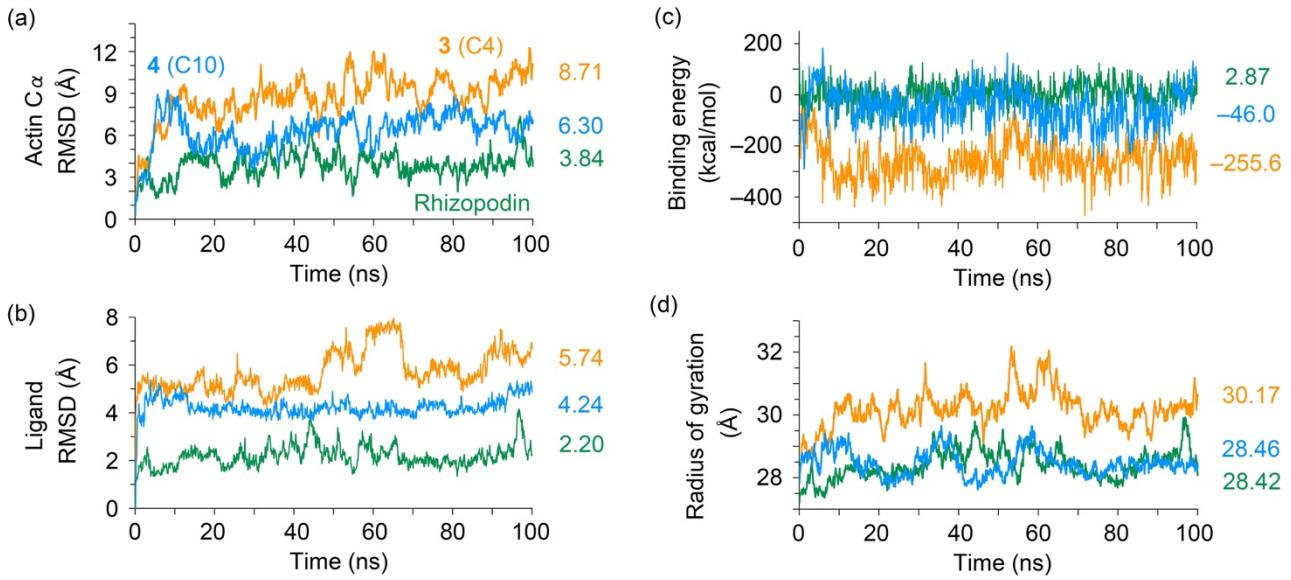

Figure S3. MD simulations of the actin–ligand complexes (rhizopodin: green, **3** (C4): orange, **4** (C10): cyan). Conformational stabilities of (a) actin and (b) ligands, (c) binding energy, and (d) radius of gyration data for protein compactness simulated at 298 K, pH 7.4 for 100 ns are summarized. Average values for 100 ns simulations are shown in the right.

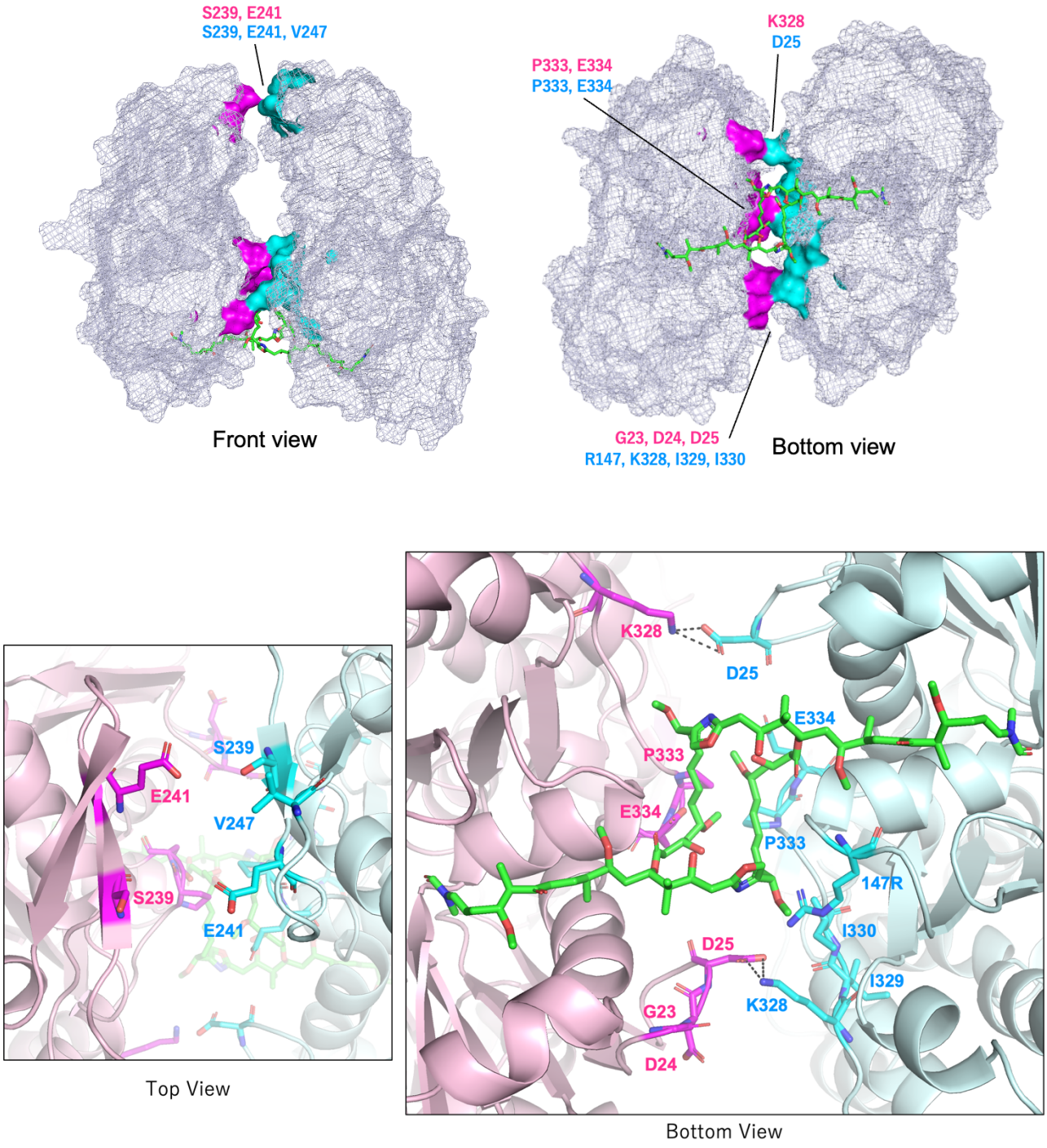

Figure S4. PPI analysis on the X-ray crystallographic structure of the original actin–rhizopodin complex [PDB: 2VYP]. Interacting residues of two actin chains are highlighted in magenta and cyan. The ligand molecules are highlighted in green stick models. Hydrogen bonds between two actin chains are shown in black dotted lines.

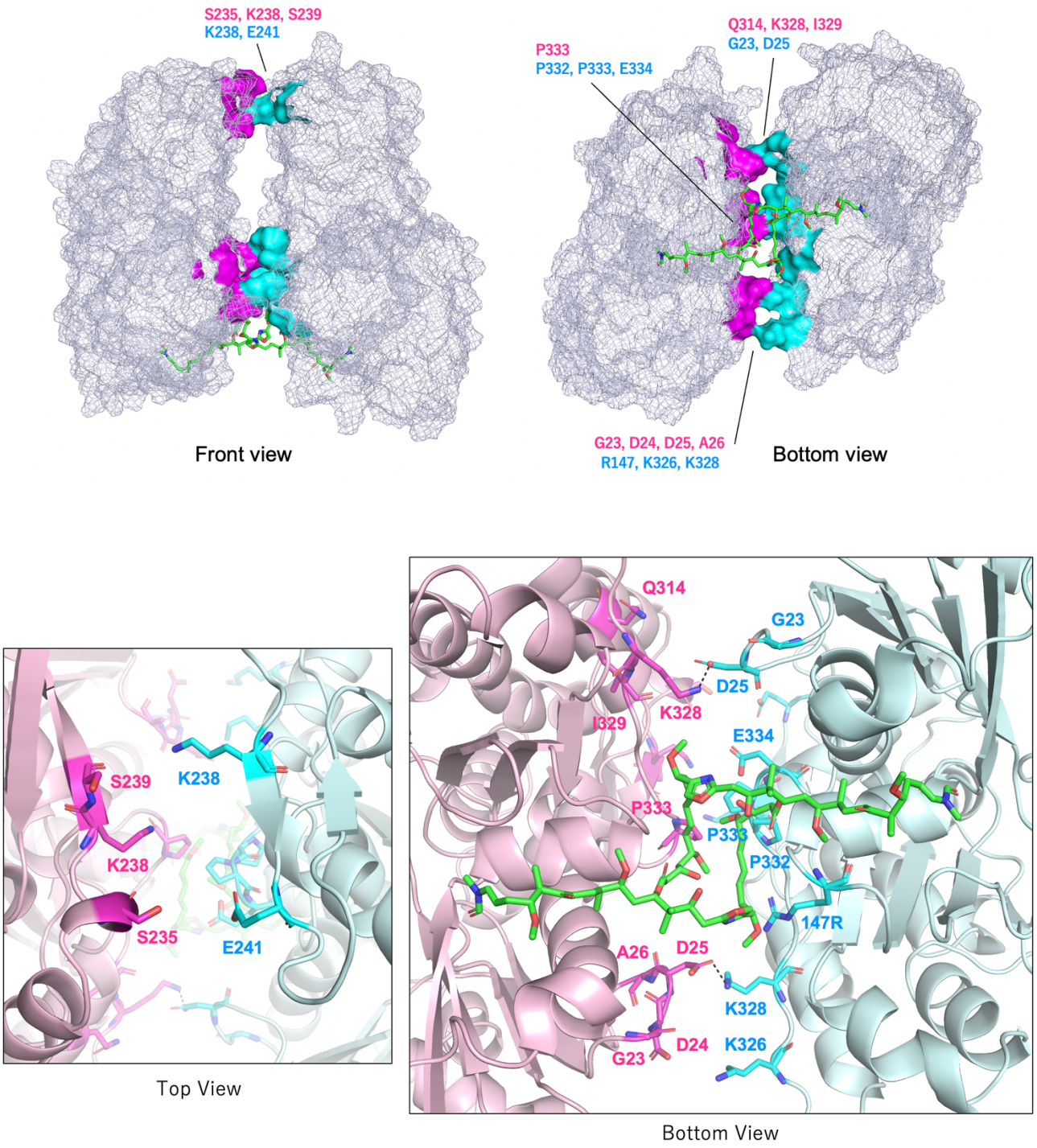

Figure S5. Structures of the actin–rhizopodin complex after MD simulation for 100 ns. Interacting residues of the chains A and B of actin are highlighted in magenta and cyan, respectively. The ligands are highlighted in green stick models. Hydrogen bonds between two actin chains are shown in black dotted lines.

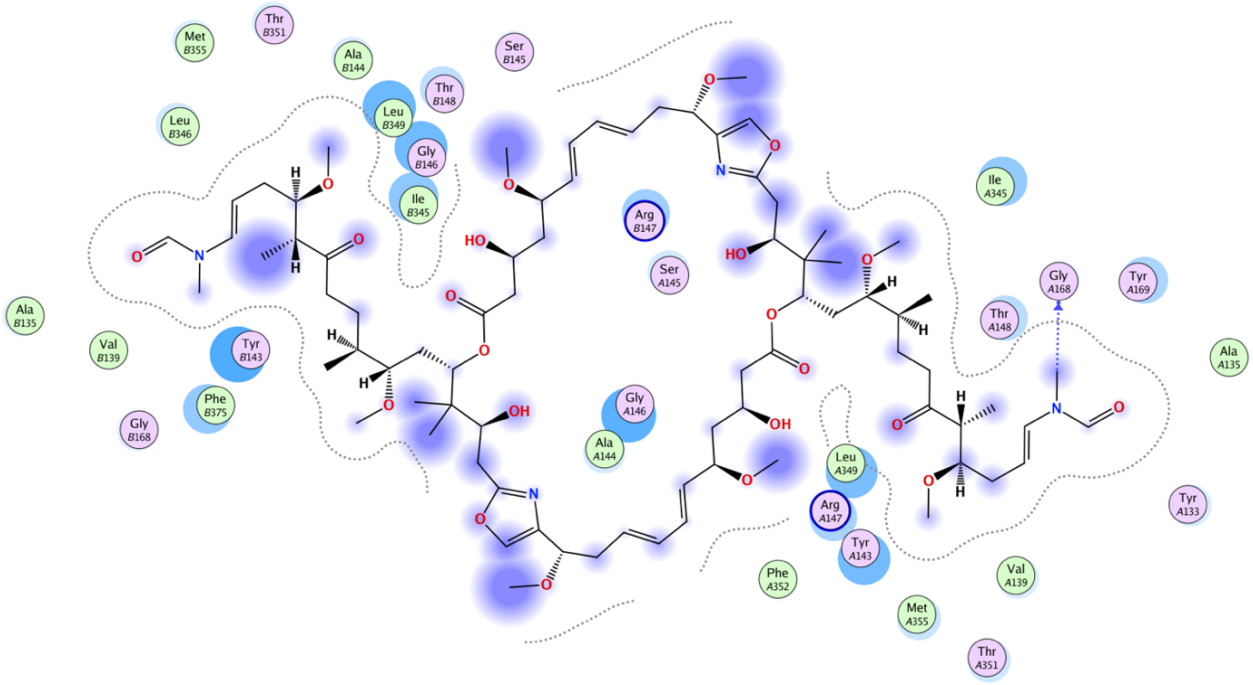

Actin–rhizopodin complex

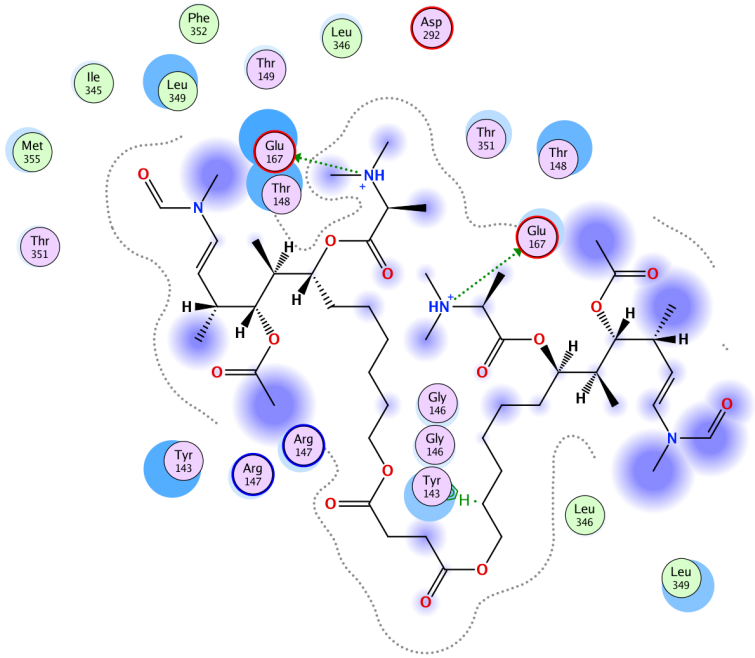

Actin–**3** complex

Figure S6. (continued)

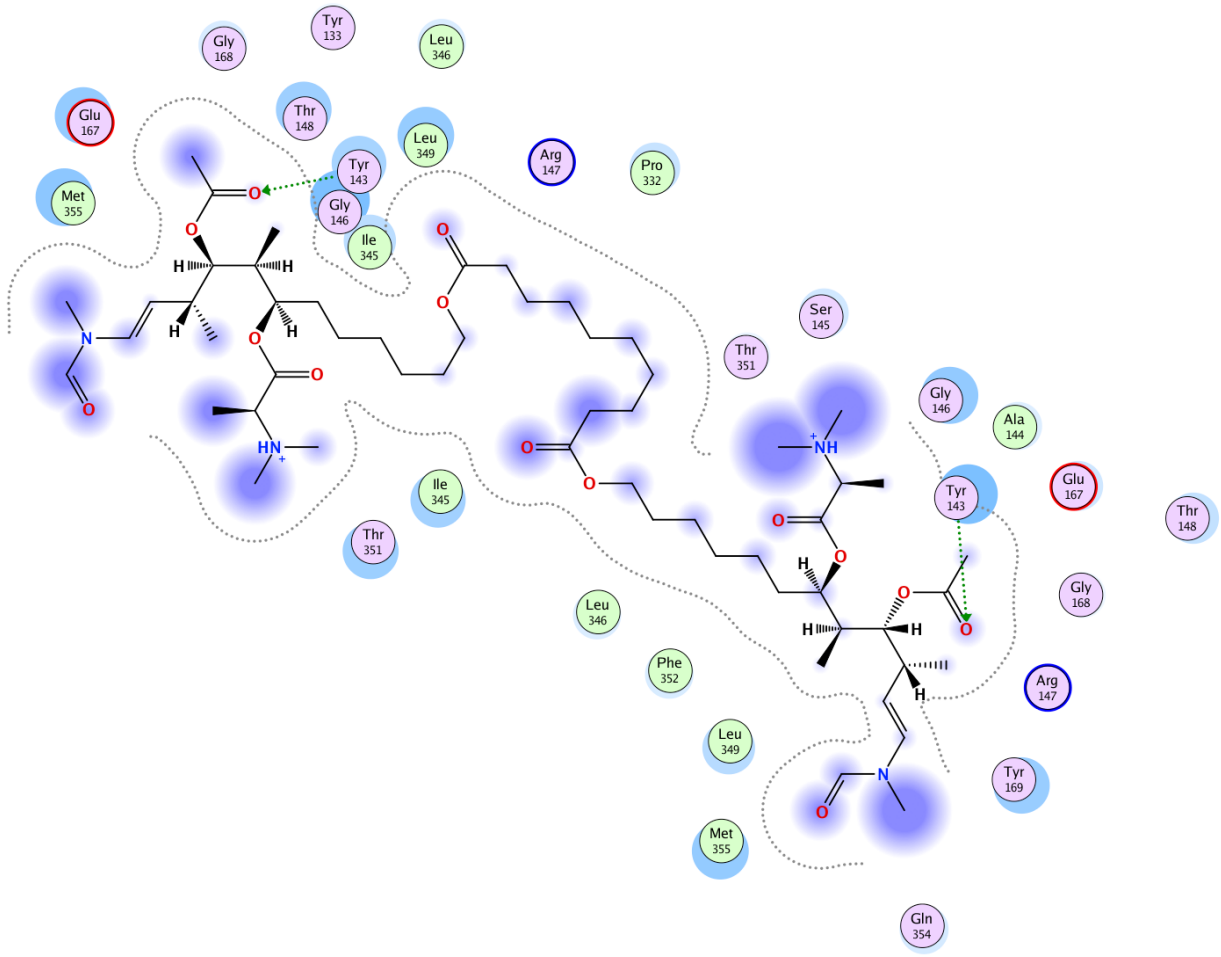

Actin–**4** complex

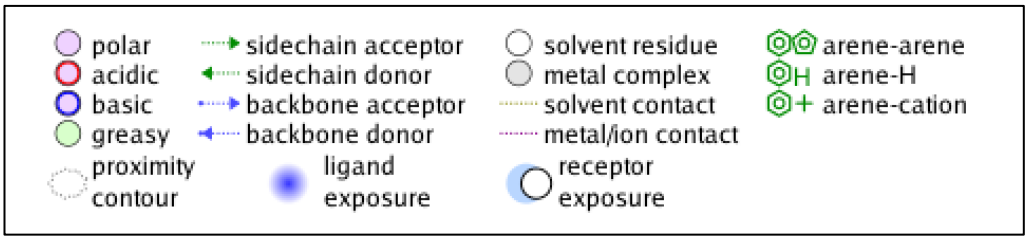

Figure S6. Protein–ligand interactions diagram analysis. Interactions of rhizopodin, C4 analog **3**, and C10 analog **4** with actin dimer proposed by MD simulation for 100 ns are summarized (see Figure 3).

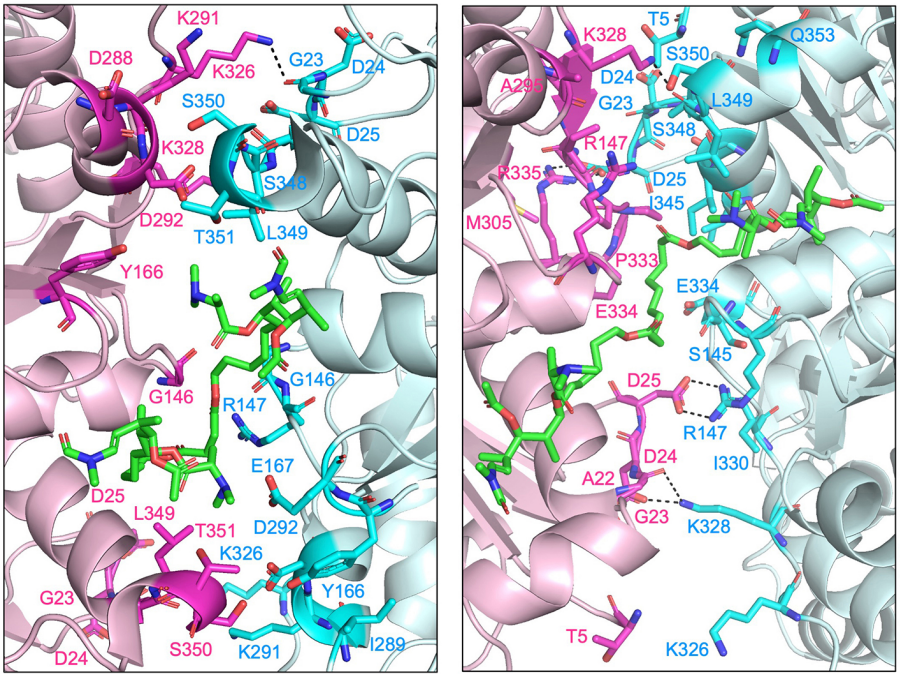

Figure S7. Structures of actin dimer complexes with **3** and **4** after MD simulation for 100 ns. Detailed views from the bottom of the interactions between actin dimers and ligands to stabilize the interfaces are shown. Interacting residues of the chains A and B of actin are highlighted in magenta and cyan, respectively. The ligands are highlighted in green stick models. Hydrogen bonds between two actin chains are shown in black dotted lines. The whole models are shown in Figure 3a.

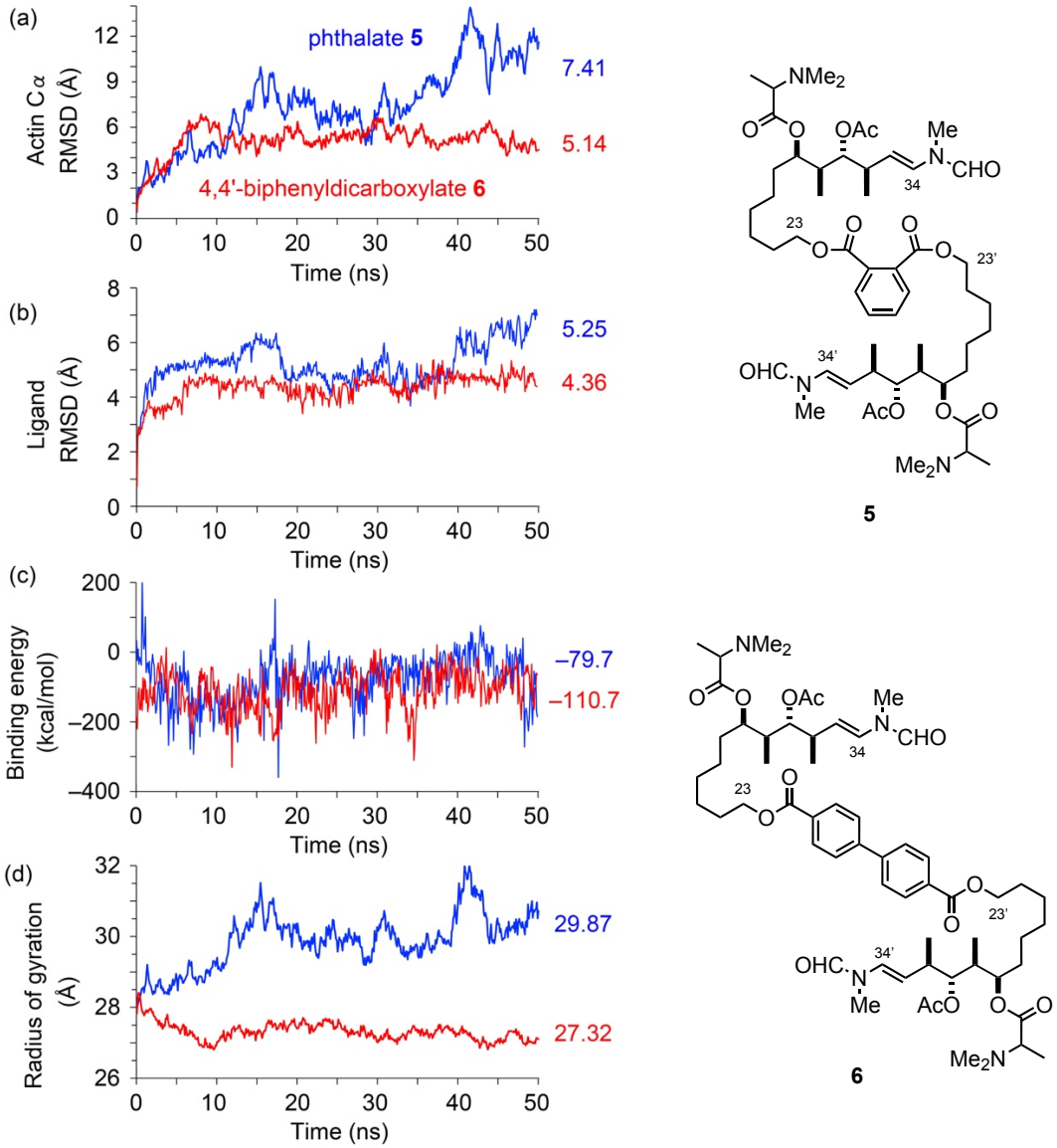

Figure S8. MD simulations of the actin–ligand complexes (phthalate **5**: blue and 4,4'-biphenyldicarboxylate **6**: red). Conformational stabilities of (a) actin and (b) ligands, (c) binding energy, and (d) radius of gyration data for protein compactness simulated at 298 K, pH 7.4 for 50 ns are summarized. Average values for 50 ns simulations are shown in the right.

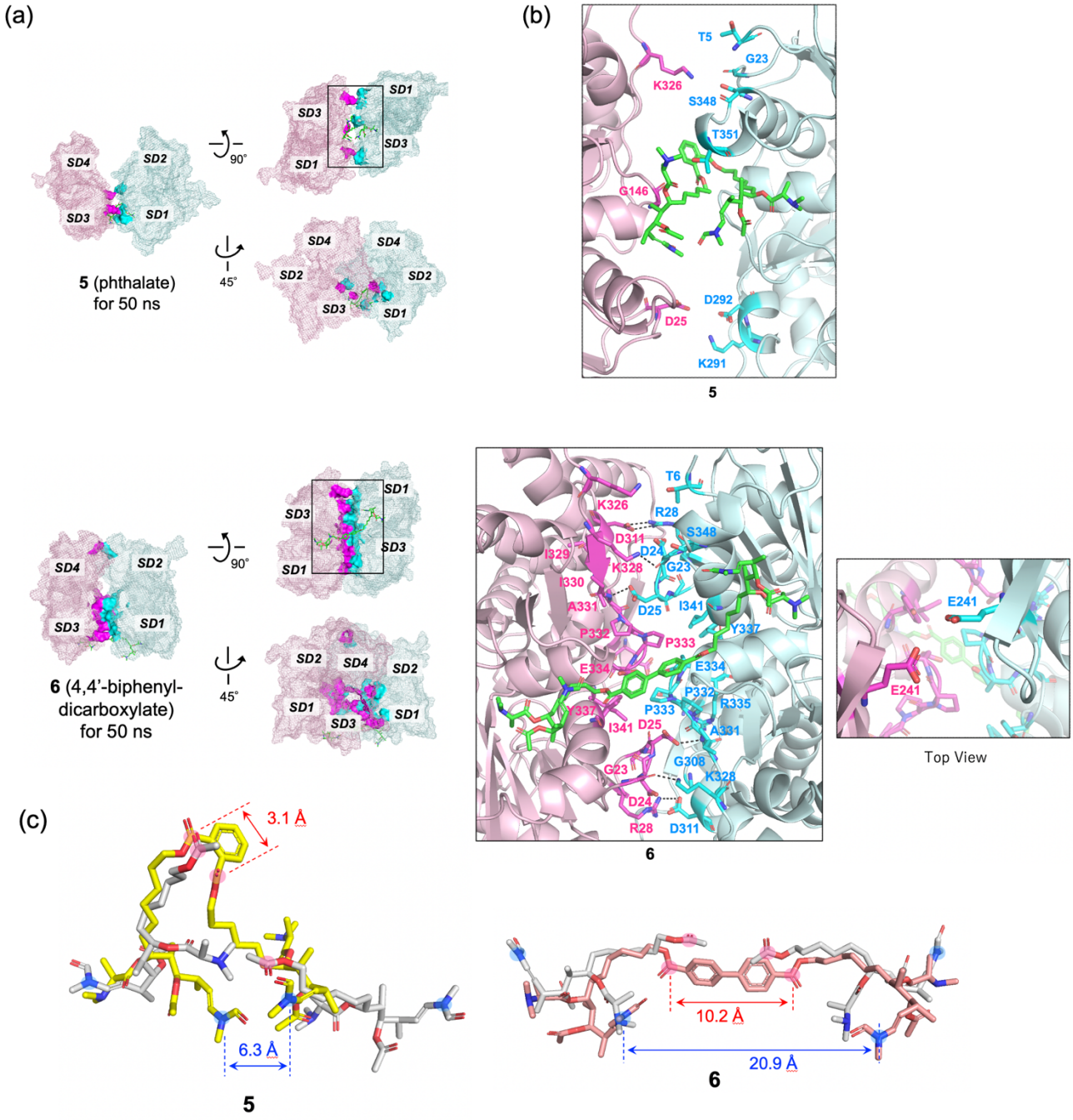

Figure S9. Structures of actin dimer complexes with phthalate **5** and 4,4'-biphenyldicarboxylate **6** after MD simulation for 50 ns. (a) PPI analysis. Interacting residues of the two actin chains are highlighted in magenta and cyan, respectively. Ligands are highlighted with green stick models. (b) Detailed views of the interactions between actin dimers and **5** or **6** to stabilize the interfaces. (c) Structures of the ligand on the actin complex. Two molecules of ligand **1** on actin (grey) obtained by molecular docking simulation using induced-fit models are superimposed. The lactone carbonyl carbon atoms and terminal enamide nitrogen atoms are highlighted with pink and blue circles, respectively. Distances between two ester C atoms or two enamide N atoms are shown.

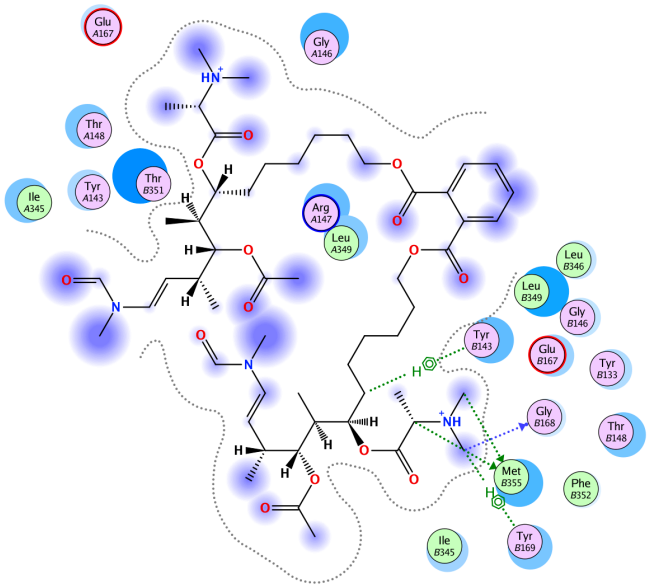

Actin–**5** complex

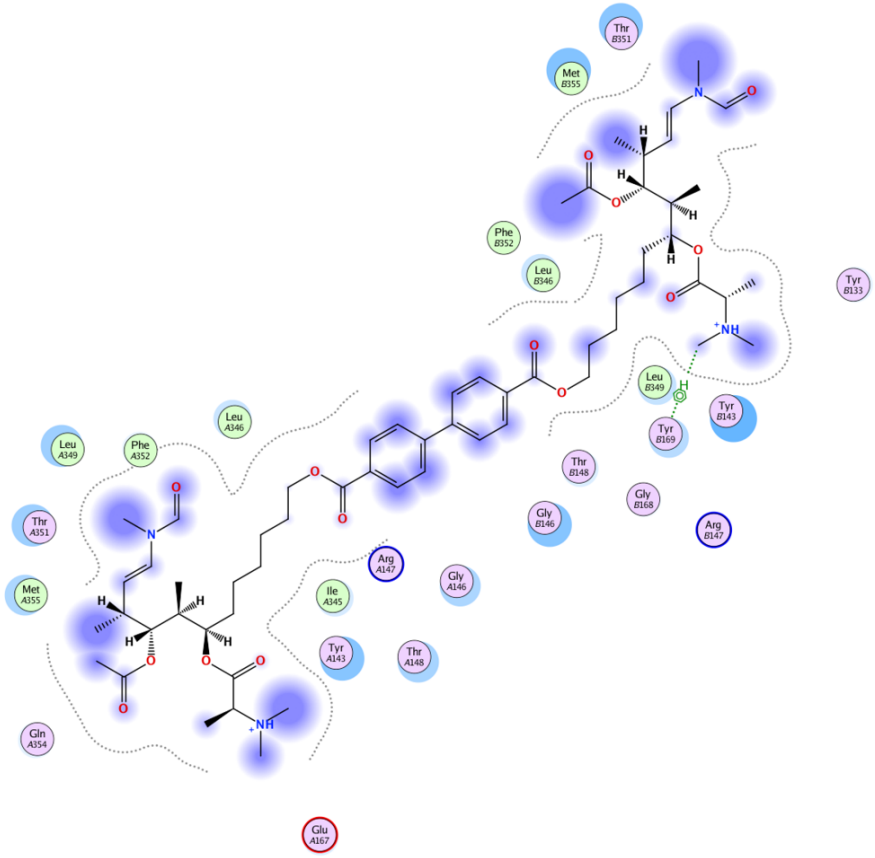

Actin–**6** complex

Figure S10. Protein–ligand interactions diagram analysis. Interactions of phthalate **5** and 4,4'-biphenyldicarboxylate **6** with actin dimer proposed by MD simulation for 50 ns are summarized (see Figure S7).

Materials and Methods

General. NMR spectra were recorded on Bruker Biospin AVANCE NEO 400 spectrometer (400 MHz for ^{1}H). Chemical shifts are reported in parts per million (ppm) relative to the solvent peak δ_H 7.26 (residual C<u>H</u>Cl$_3$). Coupling constants (*J*) are shown in hertz. High-resolution electrospray ionization mass spectra (HR-ESIMS) were measured on an Agilent 6120 TOF spectrometer. All chemicals were used as obtained commercially unless otherwise noted. An ODS silica gel COSMOSIL75C_{18}OPN (Nacalai tesque) was used for column chromatography. Merck precoated silica gel RP-18 WF_{254S} plates were used for thin layer chromatography (TLC).

Cell culture and cytotoxicity. [5c] Human colon cancer HCT-116 and embryonal kidney-derived HEK293 cells were obtained from National Institutes of Biomedical Innovation, Japan (JCRB1408 and JCRB9068) and maintained in Dulbecco's modified Eagle medium (DMEM) (with 4.5 g/L glucose) supplemented with fetal bovine serum (FBS, 10%) and Antibiotic-Antimycotic Mixed Stock Solution (100x, 1%, Nacalai tesque, Cat. 02892-54) in a humidified atmosphere with 5% CO_2 at 37 ℃. The cytotoxicity of side-chain ligands was measured by the 3-(4,5-dimethylthiazol-2-yl)-2,5-diphenyl tetrazolium bromide (MTT) method. In brief, cells were seeded at 2×10^3 cells per well in 96-well plates. After incubation overnight at 37 °C, the cells were incubated with samples for 72 h at 37°C. A 1.4 mg/mL MTT solution in phosphate buffer saline (PBS) (50 μL) was added to the cells. After 4 h, the culture medium was removed and the formazan product was dissolved in DMSO (150 μL). Optical density at 540 nm was measured with a TECAN microplate reader (Infinite® 200 Pro). All assays were performed in duplicate to confirm reproducibility.

***In vitro* F-actin sedimentation assay.** [18a] To a solution of rabbit skeletal muscle actin (3 μM, Cytoskeleton) in G-buffer [2 mM Tris·HCl (pH 8.0), 0.2 mM $CaCl_2$, 0.2 mM ATP, 0.5 mM 2-mercaptoethanol] (500 μL) was added a 0.15 M solution of $MgCl_2$ (3.3 μL), and the mixture was stirred at 25 °C for 1 h. To the polymerized F-actin solutions (200 μL) were added samples (1 μL in DMSO), and the resulting mixtures were stirred at 25 °C for 30 min and then ultracentrifuged (150,000 × *g*, 22 °C, 1 h). Aliquots of the supernatants and precipitates (re-dissolved in G-buffer) were mixed with the same amount of 2 × SDS buffer (Sigma) and boiled at 95 °C for 5 min. SDS-PAGE was performed by using a precast 10% polyacrylamide gel (ATTO), and the gels were stained with a Quick-CBB kit (Wako). Densitometry of CBB-stained proteins were performed using ImageJ software.

Gel permeation HPLC and Native PAGE analyses. Actin (50 μM, Cytoskeleton) was incubated with the ligands (ApA, 50 μM; **3**, 150 μM) at room temperature for 10 min, and the mixture was analyzed by gel permeation column chromatography on a TSKgel SuperSW3000 column (ϕ 4.6 × 300 mm, TOSOH Co.).[8a,11] The components of the mixture were eluted with a buffer consisting of 50 mM PIPES·K (pH 6.8), 100 mM KCl, and 10 mM $MgCl_2$, at 12°C, with a flow rate of 0.2 mL/min. The absorbance of the eluting solution was monitored at 280 nm. The same experiments were repeated for γ-globulin, bovine serum albumin, and actin to prepare standard curves.

HR-CN (high resolution clear native) PAGE [S3] was conducted by using the ATTO EzRun ClearNative buffer system. The same actin–ApA or actin–**3** complexes as above were used. Electrophoresis was performed using a hand-made 7.5% polyacrylamide gel, and the gels were stained with an EzStain Aqua kit (CBB stain, ATTO).

Cross-linking experiments. Actin (5 μM, Cytoskeleton) was incubated with *N*-succinimidyl 3-(3-methyl-3*H*-diazirin-3-yl)propanoate (NHS–diazirine, Cat. No. D5761, TCI Co.) (500 μM) in the absence or presence of **3** (25 μM) in G-buffer at room temperature for 20 h. The resulting mixture was irradiated with UV light (365 nm) with an LED365 benchtop spotlight (cat. LED365-SPT, 22 mW/cm^2 for 50 mm distance, OptoCode Co.) for 1 min at room temperature. SDS-PAGE was performed using a hand-made 7.5% polyacrylamide gel, and the gels were stained with an EzStain Aqua kit. This experiment was performed three times to confirm reproducibility, and a representative data are shown in Fig. 2c.

Construction of the actin–3 and actin–4 complexes and molecular modeling studies. Molecular modeling studies were performed using the Molecular Operating Environment (MOE) 2020.0901 program package (Chemical Computing Group, Inc.), similarly as described previously.[18a] For docking model studies, all water molecules associated with the actin–rhizopodin complex (PDB: 2VYP) were removed, except for those near the ligand, and all protons on the protein and the ligand were complemented. On the docking simulations of the actin–**3**, –**4** , –**5**, and –**6** complexes, the actin structures in two sets of the actin–**1** complex models [19] were superimposed on those in the actin–rhizopodin complex. The terminal acetyl groups in **1** were replaced with the C4 and C10 alkyl diesters for **3** and **4**, and phthalate and 4,4'-biphenyldicarboxylate for **5** and **6**, respectively. By using these models as initial structures, conformational searches were performed using the Amber14:EHT force-field with GB/VI Generalized Born [S1] implicit solvent electrostatics (D_{in} = 1, D_{out} = 80) and with LowModeMD, in which the binding site of **1** on actin was settled as the ligand-binding site. Refinements were performed using the rigid-body model, and the lowest conformation models in energy (or the third most stable model for **6**) were used for further MD simulation studies.

Molecular dynamics simulation. [12a] Molecular dynamics (MD) simulations were performed for the actin and rhizopodin, **3**–**6** complexes using YASARA (21.12.19) software to evaluate the conformational stability of proteins and ligands.[S2] The actin–ligand complexes were inserted into a cubic box of water molecules, with a density of 0.997 g/mL and a temperature of 298 K. We used 0.9% NaCl (physiological solution) and a default physiological pH at 7.4. The simulation was performed at a normal speed (2 × 1.25 fs timestep). After the steepest descent and simulated annealing minimizations, a simulation was run for 50 or 100 ns using the AMBER14 Force Field. The water molecules were described by the TIP3P model. Periodic boundary conditions were applied. All protein structural data were represented in cartoon and surface model, while ligand was showed as sphere or stick model. MOE and PyMol (Molecular Graphics System, Version 2.0 Schrödinger, LLC) were used for final image processing which suitable for scientific representation. The interacted residues of actin with rhizopodin, **3**, and **4** were visualized with MOE.

Synthesis and spectroscopic data of side-chain ligands.

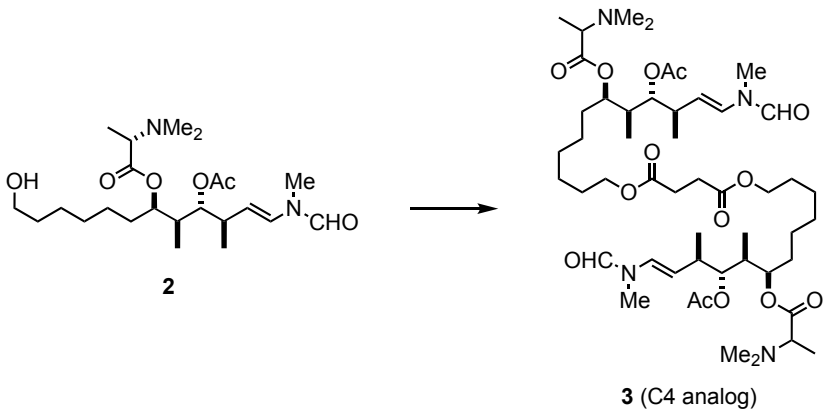

C4 analog 3. To a stirred solution of primary alcohol **2** (2.9 mg, 6.6 μmol) [19] and succinic acid (0.39 mg, 3.3 μmol) in dry CH_2Cl_2 (0.1 mL) were added EDC·HCl (3.8 mg, 20 μmol) and 4,4'-dimethylaminopyridine (DMAP) (0.24 mg, 2.0 μmol). After stirring at room temperature for 20.5 h, the resulting mixture was diluted with CH_2Cl_2 (5 mL), and washed with sat. $NaHCO_3$ aq. (7.5 mL × 2) and brine, dried with Na_2SO_4, and concentrated. The crude material was purified with an ODS column chromatography [COSMOSIL75C_{18}OPN 0.1 g ($CHCl_3$ / MeOH = 1:1)] and a reversed-phase HPLC [Develosil ODS-HG-5 (ϕ 20 x 250 mm), 75% MeOH / 25% 20 mM NH_4OAc aq., 5 mL/min, 254 nm] to afford C4 analog **3** (0.81 mg, 26%) as a colorless oil. **3**: R_f 0.45 (ODS, $CHCl_3$/MeOH = 1:1); ^{1}H NMR (400 MHz, $CDCl_3$) δ 8.29 [8.08] (s, 2H), 6.49 [7.15] (d, J = 14.0 Hz, 2H), 5.02 (m, 2H), 4.97 (dd, J = 14.5, 8.6 Hz, 2H), 4.77 (dd, J = 9.9, 2.8 Hz, 2H), 4.06 (t, J = 6.7 Hz, 4H), 3.21 <3.24> (q, J = 7.9 Hz, 2H), 3.03 [3.07] (s, 6H), 2.61 (s, 4H), 2.55 (m, 2H), 2.37 <2.35> (s, 12H), 2.08 <2.07> (s, 6H), 1.80 (m, 2H), 1.67–1.57 (m, 4H), 1.43 (m, 2H), 1.35–1.20 (m, 14H), 1.30 <1.28> (d, J = 7.2 Hz, 6H), 1.02 [1.01] (d, J = 6.9 Hz, 6H), 0.94 (d, J = 6.9 Hz, 6H), Chemical shifts of the minor rotamer at the *N*-methylenamide moiety (1.9/1) and DMAla (*S*/*R* = 2.5/1) are within parentheses (square and angle blankets, respectively); HRMS (ESI) *m/z* 967.6197 (calcd for $C_{50}H_{87}N_4O_{14}$ $[M+H]^+$, Δ –1.7 mmu).

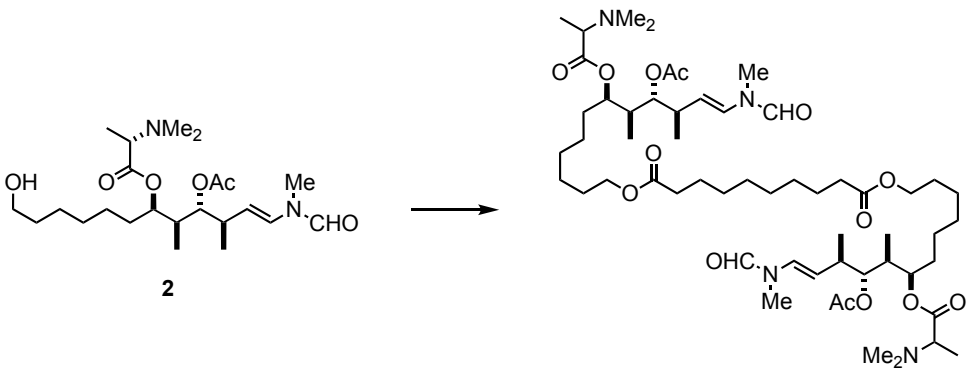

C10 analog 4. To a stirred solution of primary alcohol **2** (3.0 mg, 6.8 μmol) and sebacic acid (0.69 mg, 3.4 μmol) in dry CH_2Cl_2 (0.1 mL) were added EDC·HCl (3.8 mg, 20 μmol) and 4,4'-dimethylaminopyridine (DMAP) (0.24 mg, 2.0 μmol). After stirring at room temperature for 5.5 h, the resulting mixture was diluted with CH_2Cl_2 (5 mL), and washed with sat. $NaHCO_3$ aq. (5 mL × 2) and brine, dried with Na_2SO_4, and concentrated. The crude material was purified with an ODS column chromatography [COSMOSIL75C_{18}OPN 0.4 g ($CHCl_3$ / MeOH = 1:1)] and a reversed-phase HPLC [Develosil ODS-HG-5 (ϕ 20 x 250 mm), 85% MeOH / 15% 20 mM NH_4OAc aq., 5 mL/min, 254 nm] to afford C10 analog **4** (1.2 mg, 32%) as a colorless oil. **4**: R_f 0.32 (ODS, $CHCl_3$/MeOH = 1:1); ^{1}H NMR (400 MHz, $CDCl_3$) δ 8.29 [8.08] (s, 2H), 6.49 [7.15] (d, *J* = 14.1 Hz, 2H), 5.03 (m, 2H), 4.97 (dd, *J* = 14.0, 9.3 Hz, 2H), 4.77 (dd, *J* = 9.8, 3.0 Hz, 2H), 4.04 (t, *J* = 6.8 Hz, 4H), 3.22 <3.24> (q, *J* = 7.1 Hz, 2H), 3.03 [3.07] (s, 6H), 2.55 (m, 2H), 2.37 <2.35> (s, 12H), 2.27 (t, *J* = 7.4 Hz, 4H), 2.08 <2.07> (s, 6H), 1.82 (m, 2H), 1.67–1.57 (m, 8H), 1.43 (m, 2H), 1.37–1.20 (m, 22H), 1.30 <1.28> (d, *J* = 7.2 Hz, 6H), 1.02 [1.01] (d, *J* = 6.9 Hz, 6H), 0.94 (d, *J* = 7.0 Hz, 6H), Chemical shifts of the minor rotamer at the *N*-methylenamide moiety (1.9/1) and DMAla (*S*/*R* = 3.5/1) are within parentheses (square and angle blankets, respectively); HRMS (ESI) *m/z* 526.3603 (calcd for $C_{56}H_{100}N_4O_{14}$ $[M+2H]^{2+}$, Δ –1.0 mmu).

NMR spectra

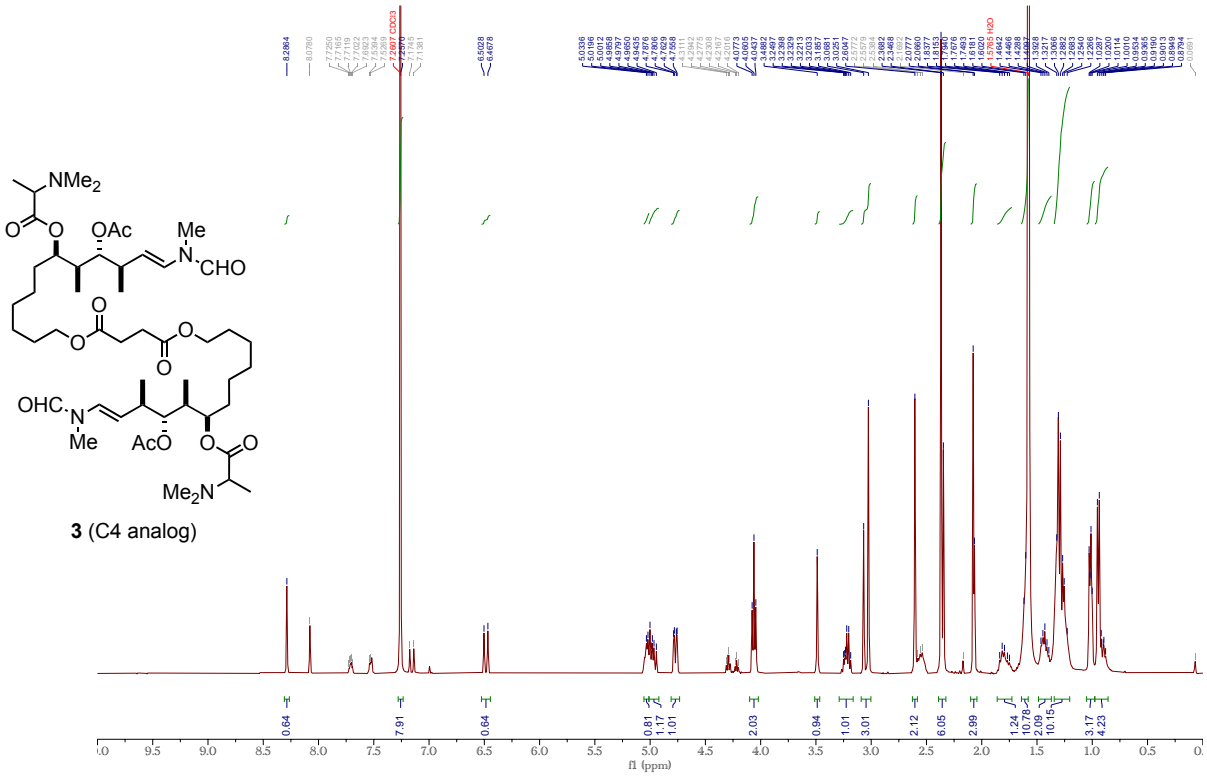

^{1}H NMR spectrum of **3** (400 MHz, CD_3OD).

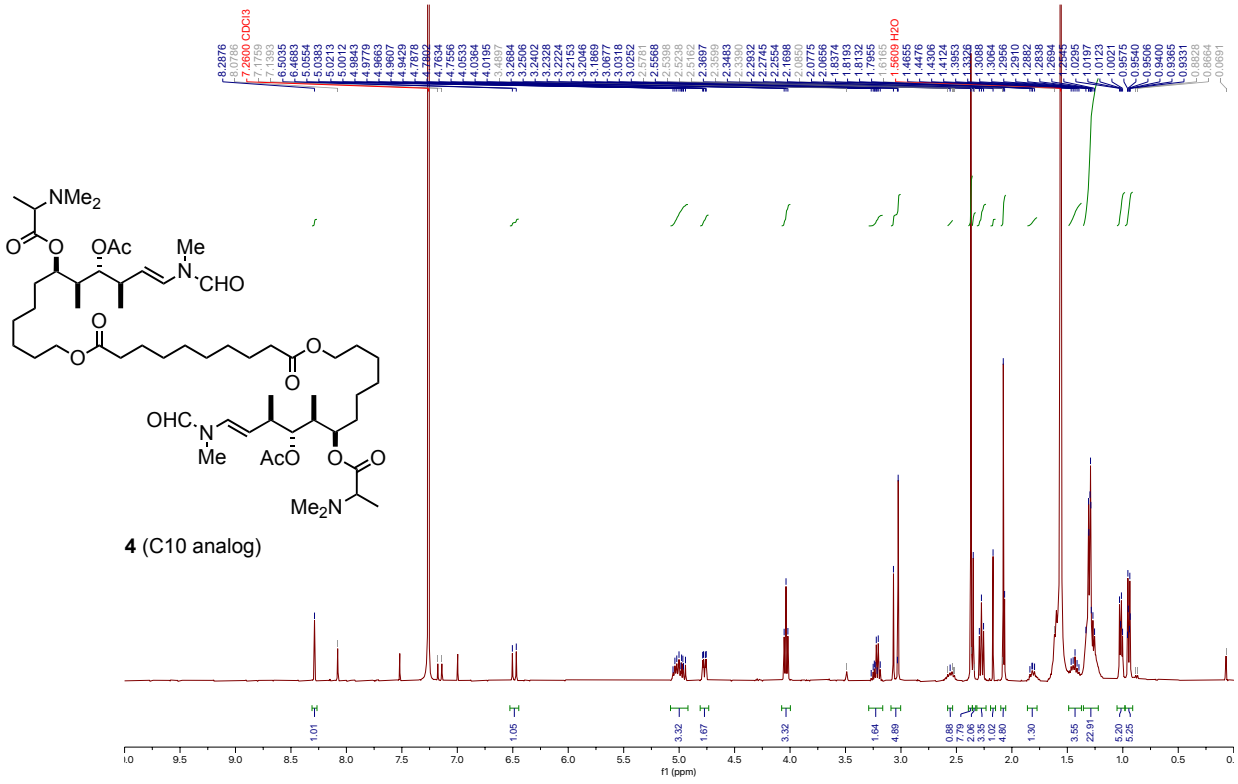

^{1}H NMR spectrum of **4** (400 MHz, CD_3OD).

HPLC charts

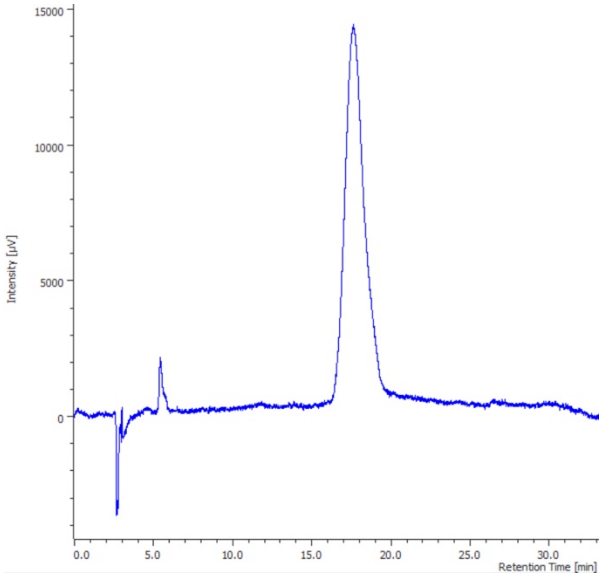

C4 dimer analog **3**.

Develosil ODS-HG-5 (Φ 4.6 × 250 mm), 75% MeOH / 25% 20 mM NH_4OAc, 1.0 mL/min, 25 ºC, UV 254 nm, t_R 17.6 min

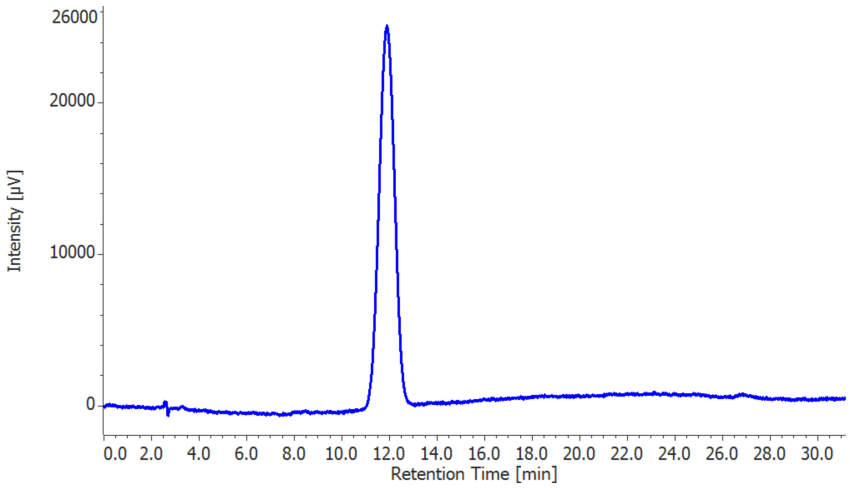

C10 dimer analog **4**.

Develosil ODS-HG-5 (Φ 4.6 × 250 mm), 85% MeOH / 15% 20 mM NH_4OAc, 1.0 mL/min, 25 ºC, UV 254 nm, t_R 11.9 min

Original gel images

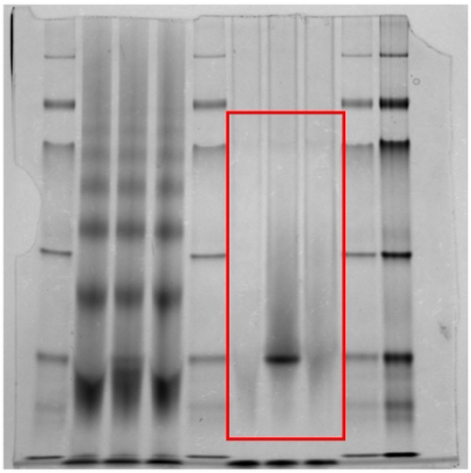

Figure 2B

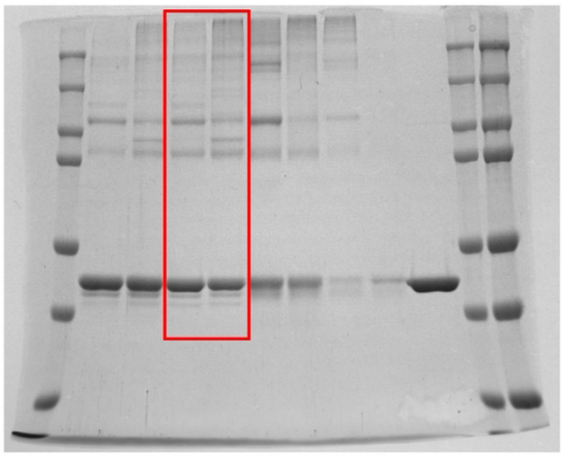

Figure 2C

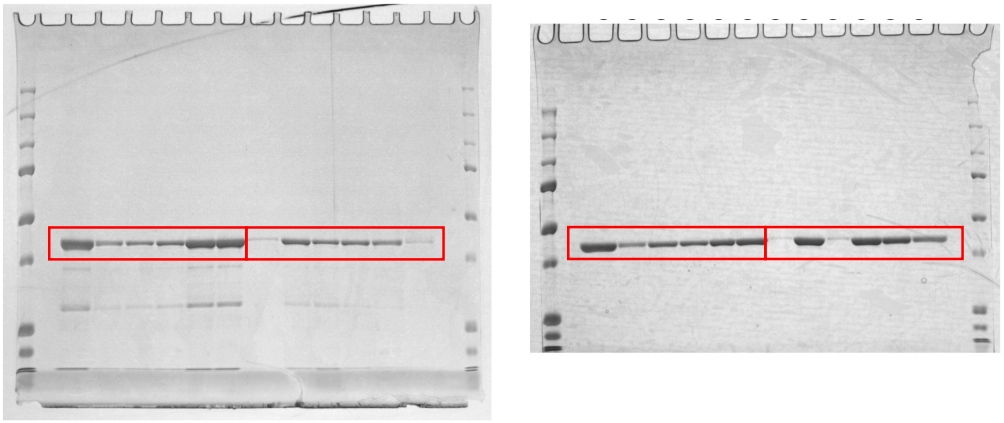

Figure S1

References

S1 P. Labute, *J. Comput. Chem.*, 2008, **29**, 1693.

S2 H. Land and M. S. Humble, *Methods Mol. Biol.*, 2018, **1685**, 43.

S3. I. Wittig, M. Karas and H. Schägger, *Mol. Cell Proteomics*, 2007, **6**, 1215.